

Eliminating unobservable parameters in physics models using deep learning

C. H. Kim,¹ K. Y. Chae,^{1,*} M. S. Smith,² D. W. Bardayan,³ C. R. Brune,⁴ R. J. deBoer,³ D. Lu,⁵ and D. Odell⁴

¹*Department of Physics, Sungkyunkwan University, Suwon 16419, Republic of Korea*

²*Physics Division, Oak Ridge National Laboratory, Oak Ridge, TN, 37831, USA*

³*Department of Physics, University of Notre Dame, Notre Dame, IN, 46556, USA*

⁴*Department of Physics and Astronomy, Ohio University, Athens, OH, 45701, USA*

⁵*Computational Sciences and Engineering Division,
Oak Ridge National Laboratory, Oak Ridge, TN, 37831, USA*

Physics models typically contain adjustable parameters to reproduce measured data. While some parameters correspond directly to measured features in the data, others are unobservable. These unobservables can, in some cases, cause ambiguities in the extraction of observables from measured data, or lead to questions on the physical interpretation of fits that require these extra parameters. We propose a method based on deep learning to extract values of observables directly from the data without the need for unobservables. The key to our approach is to label the training data for the deep learning model with only the observables. After training, the deep learning model can determine the values of observables from measured data with no ambiguities arising from unobservables. We demonstrate this method on the phenomenological R-matrix that is widely utilized in nuclear physics to extract resonance parameters from cross section data. Our deep learning model based on Transformers successfully predicts nuclear properties from measurements with no need for the channel radius and background pole parameters required in traditional R-matrix analyses. Details and limitations of this method, which may be useful for studies of a wide range of phenomena, are discussed.

Models are routinely used to understand physical systems by fitting their predictions to measurement data and extracting “best fit” values for the model parameters. In some cases, these parameters correspond directly to system observables, i.e., features that can be measured. In other cases, the parameters do not correspond to measurable features, but rather may codify approximations made in the model or may be part of the framework of the model itself. The presence of these unobservable parameters can, in some cases, lead to ambiguities in the extraction of observables from measured data or lead to questions on the physical interpretation of fits that require these extra parameters [1–3]. When possible, it is advantageous to extract values of observable parameters directly from features in the data without the need for unobservables.

One of the strengths of deep learning is the ability to identify features in data sets. For this reason and others, deep learning has been successfully used in a variety of science fields [4–12]. In this study, we propose to use deep learning to extract values of observable parameters directly from measured data sets, bypassing the need for unobservable parameters that can introduce ambiguities or increase uncertainties in the results. Fig. 1 shows a sketch of the method. First, training data is generated by running a physics model \mathcal{P} with various combinations of the observable θ_{obs} and unobservable θ_{un} parameter inputs. These outputs can be processed with a noise function \mathcal{N} to simulate the noise present in experimental measurements. Then, a deep learning model (neural network) \mathcal{D} is trained on this data to find particular ob-

servable features in the output of the physics model \mathcal{M} . The key to our method is to label the training data with *only* the observable parameter values, so that the deep learning model finds the features without any knowledge of the unobservable parameters. After training, the deep learning model \mathcal{D} is used to directly determine observable parameters θ_{obs} from measured data \mathcal{M} with no ambiguities arising from unobservable parameters.

We demonstrate this method on the phenomenological R-matrix that is being critically used in nuclear physics [1, 3, 13–19]. The phenomenological R-matrix serves as a good example because it contains numerous and somewhat arbitrary unobservable parameters. It is based on separating the particle interaction space into internal and external regions. The complex many-body nuclear interactions are present in the internal region, whereas only the Coulomb interaction is considered in the external region. The boundary surface is defined by a sphere of radius known as the channel radius. The internal interactions are described by the R-matrix that is characterized by parameters of nuclear resonant states. From the R-matrix, expected observational data such as cross sections can be calculated. The parameters of nuclear states are determined by comparing the expected and experimental data. The extracted parameters provide the related nuclear properties, and the cross sections can be reproduced using the parameters for the purpose of extrapolation.

The main drawback of the phenomenological R-matrix arises from the dependency of fitted physical parameters on rather arbitrary choices of unobservable parameters [1, 3]. The R-matrix theory requires an infinite number of nuclear states in the calculation. However, the truncation of the number of states is necessary for the phe-

* kchae@skku.edu; Fax: +82-31-290-7055

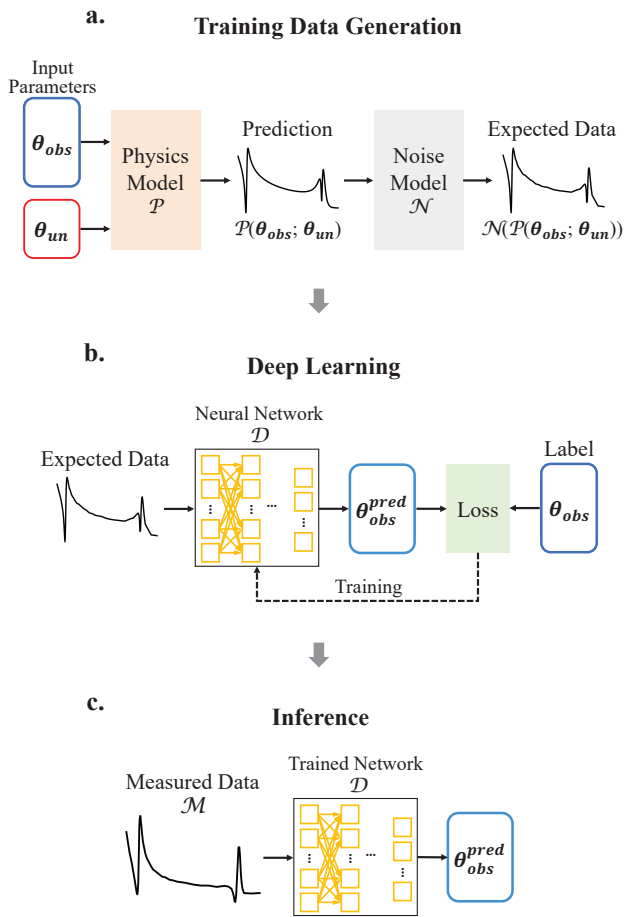


FIG. 1. Process of the current method to eliminate the unobservable parameters. The current method starts from (a) training data generation for (b) deep learning modeling to (c) inference on target measurement. The model requires only measurement data to extract physical objects at the inference stage.

nomenological approach, as generally only a limited number of nuclear states are known. The truncated states are compensated by the so-called background poles that are artificial states included to reproduce the effects of the truncated states. The strength of the background poles depends on the channel radius, which creates additional complications [1, 3, 13]. In practice, there are no strict physics rules to select valid choices of the channel radius and background poles. Different choices produce different fitting results because they create different theoretical predictions. This feature has caused difficulties in the phenomenological analysis and uncertainties of the results [1, 3].

We utilize the proposed method to extract observables without the requirement of unobservables used in the phenomenological R-matrix. One of the important applications of the phenomenological R-matrix is determining resonance parameters (e.g., spins J , parities π , energies E , widths Γ) in nuclear reaction data. We built a deep

TABLE I. Training data distribution and test results of model. Model performance is presented with accuracy and mean errors. Median values are taken to calculate the errors. The values in the parentheses are percentage errors. In total, 5 BGPs are included.

Parameters	Data Distribution	Model Performance
J_1^π	$\frac{1}{2}^+$ (Fixed)	J : -, π : -
J_2^π	$l \leq 2$	J : 98.6 %, π : 100.0 %
J_3^π	$l = 2$	J : 99.0 %, π : -
E_1 (MeV)	Normal(0.425, 0.003)	0.00014 (0.03 %)
E_2 (MeV)	Normal(1.565, 0.010) ³	0.00118 (0.08 %)
E_3 (MeV)	Normal(1.610, 0.006) ³	0.00057 (0.04 %)
Γ_1 (keV)	Normal(30, 3)	0.20 (0.67 %)
Γ_2 (keV)	Normal(50, 15)	1.98 (4.44 %)
Γ_3 (keV)	Normal(60, 8)	1.23 (2.08 %)
ANC (fm ^{-1/2}) ¹	Normal(1.81, 0.07)	-
a_c (fm)	3 - 8	-
5 BGPs [J^π]	$l \leq 2$	-
5 BGPs [E]	Uniform(3, 10)	-
5 BGPs [Γ]	Uniform(0, Γ_W) ²	-

¹ Asymptotic normalization coefficient (ANC) for the subthreshold state is also included in the R-matrix calculation but not as one of the objects to simplify the demonstration. The range is taken from the previous study [16, 20].

² Γ_W is the proton width calculated from $\Gamma_W = 2P\gamma_W^2 = 2P(3\hbar^2/2\mu a_c^2)$, where P is the penetrability, γ_W^2 is the Wigner limit, and μ is the reduced mass. ³ We set E of second and third states to be separated more than 10 keV as the energy bin sizes of the measurement data in this region are ≥ 10 keV.

learning model to find patterns of resonance parameters in reaction cross section spectra. Specifically, our goal was to extract the parameters of three resonance states from the well-known $^{12}\text{C}+p$ elastic scattering measurement of ref. [21] without using any information on the channel radius and background poles.

The training data for this task was prepared by the following specific process. We sampled possible sets of resonance parameters, along with a random value of the channel radius (a_c) and a random configuration of background poles (BGPs). We assumed a general situation where previous studies have partly determined the resonance parameters. Table I shows the training data distributions of the parameters. Here, l is the relative orbital angular momentum of the particle pair. Possible spins and parities with the given l were uniformly sampled: e.g., $J = 0.5 - 2.5$ and $\pi = +, -$ for $l \leq 2$. We set the range of the channel radius to 3-8 fm that contains

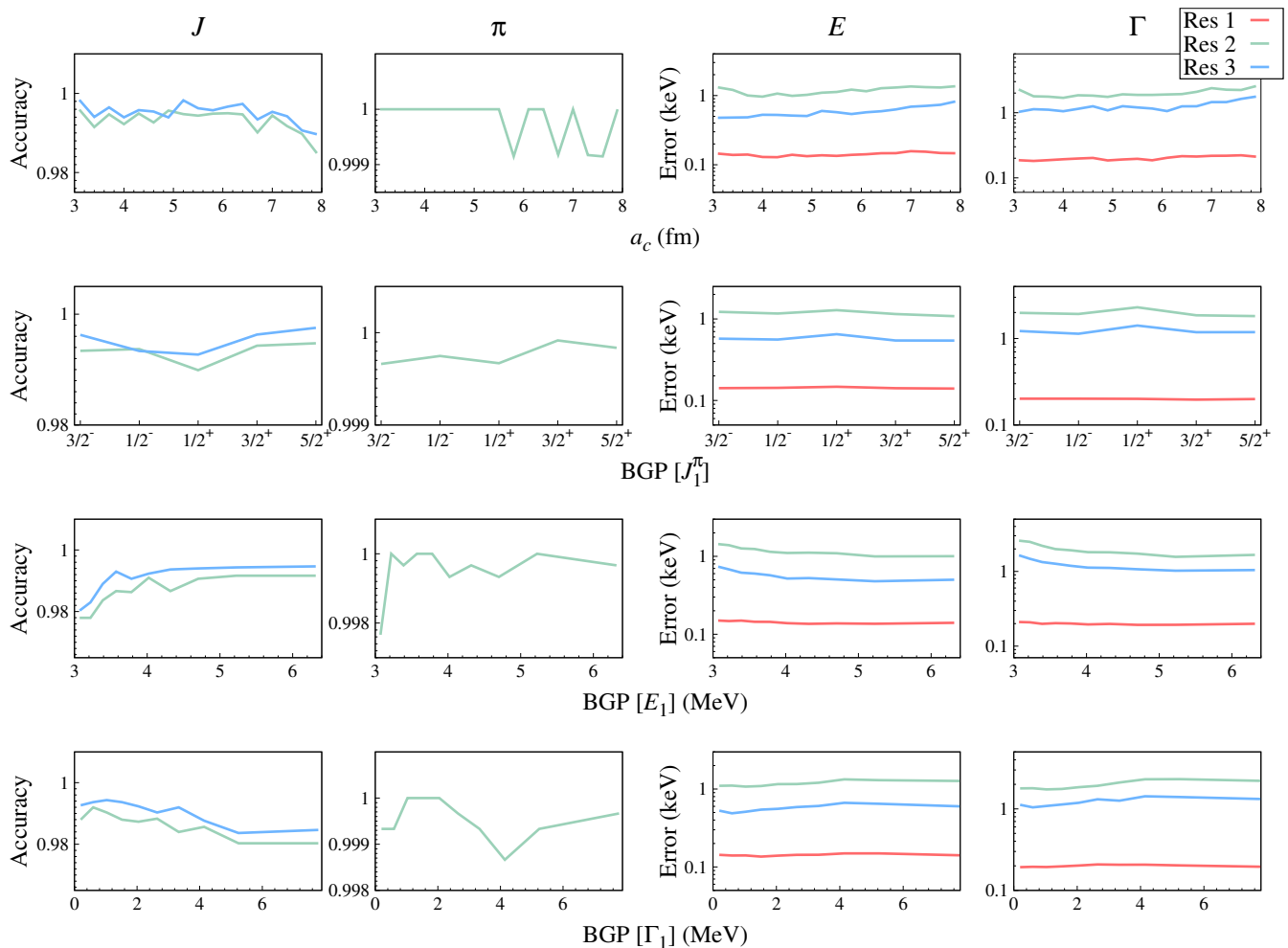


FIG. 2. Errors of the model predictions for cross sections calculated with various unobservables. Res 1, 2, and 3 represent the first, second, and third resonances. The figures of the first background pole are given as representations.

typical values being used in traditional R-matrix calculations. A level for each possible spin-parity was included as a background pole. The location and width of these levels were randomly determined within the given ranges.

We calculated cross section spectra corresponding to each set of parameters using R-matrix theory [16]. As the calculated spectra do not carry experimental noise, we added random noise to the spectra to reflect the measurement errors given by ref. [21]. We gave the log of the differential cross sections as the inputs to the model, while the labels are the corresponding values of parameters J , π , $\log(E)$, and $\log(\Gamma)$ of three resonance states.

Transformers are currently one of the most effective deep learning architectures in a variety of applications [22–28]. We modify a Transformer to be suitable for this task. Details of the implemented architecture are described in the Methods section. Here, we summarize the primary specifications: First, as the input data are differential cross section spectra at three different angles, an extra dimension for the angles is needed in addition to the 2-dimensional cross section spectrum. Relations

between the spectra of different angles are important in the analysis. However, Transformers consist of matrix multiplications that are operated only at the last two dimensions and are therefore limited within a spectrum at each angle. To accommodate this, we replaced the decoder input with the encoder input that is shifted in the angle dimension. By doing so, the matrix multiplications in the decoder are also operated between spectra at different angles. Second, because the different nature of our four parameters J , π , E , and Γ , we split the model output into four branches where two of them predict discontinuous values (classification) for J and π , and the others predict continuous values (regression) for E and Γ .

Using deep ensembles, probabilistic deep learning is also used to quantify uncertainties of model predictions [29–31]. The idea of deep ensembles is straightforward and highly effective, featuring the use of point-estimate models which are trained, using a negative log-likelihood loss function, from random initial model parameters and shuffled data samples [29, 32, 33]. The model predic-

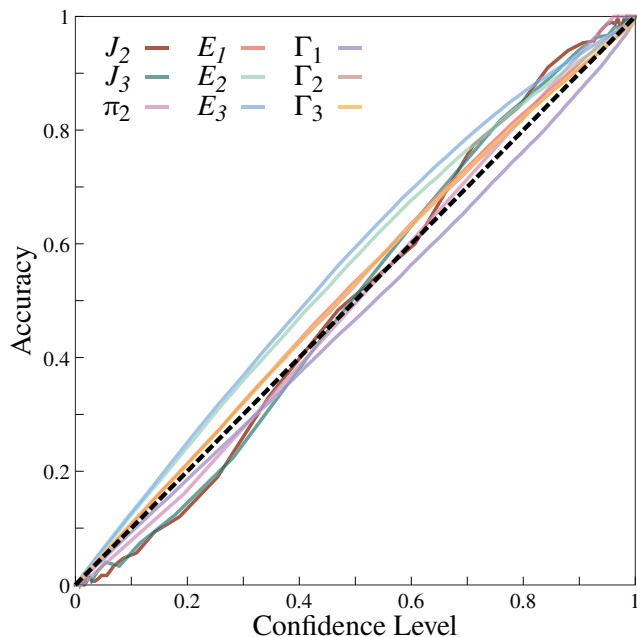


FIG. 3. Reliability diagram of the current model. Each curve shows the estimated accuracy (fraction of true data points included in the confidence range) as a function of the corresponding confidence level. It is the standard method to evaluate the calibration of uncertainty predictions.

tion \mathbf{y} on given input data \mathbf{x} can be obtained from the predictions of these multiple models:

$$p(\mathbf{y}|\mathbf{x}) = \frac{1}{N_{\text{model}}} \sum_{n=1}^{N_{\text{model}}} p(\mathbf{y}|\mathbf{x}, \theta_n), \quad (1)$$

where θ_n represents parameters of the n th model. The predictive probability for the classification of J or π is, therefore, the average of the probabilities predicted by the models. For the regression of $\log(E)$ or $\log(\Gamma)$, we assume that the likelihoods $p(\mathbf{y}|\mathbf{x}, \theta)$ follow Gaussian distributions. The predictive distribution $p(\mathbf{y}|\mathbf{x})$ is further approximated as a Gaussian for simplicity, where its mean and variance are those of the mixture of the Gaussian likelihoods [31]. The final distribution is equivalent to the lognormal distribution of E or Γ , which has several well-known advantages for representing positive-definite quantities [34]. More details of deep ensembles and the training process are presented in the Methods section.

The last column in Table I shows the average accuracies and errors of the trained model on the test dataset. The results show that the method and current model are quite effective. Fig. 2 shows errors of the predicted parameters for cross sections calculated with different values of eliminated parameters. The model predictions display little dependence – less than $\sim 2\%$ and ~ 1 keV for classification and regression, respectively – on these parameters within the training data distribution; as with any deep learning application, the model performance is not guaranteed outside of this range. By using more

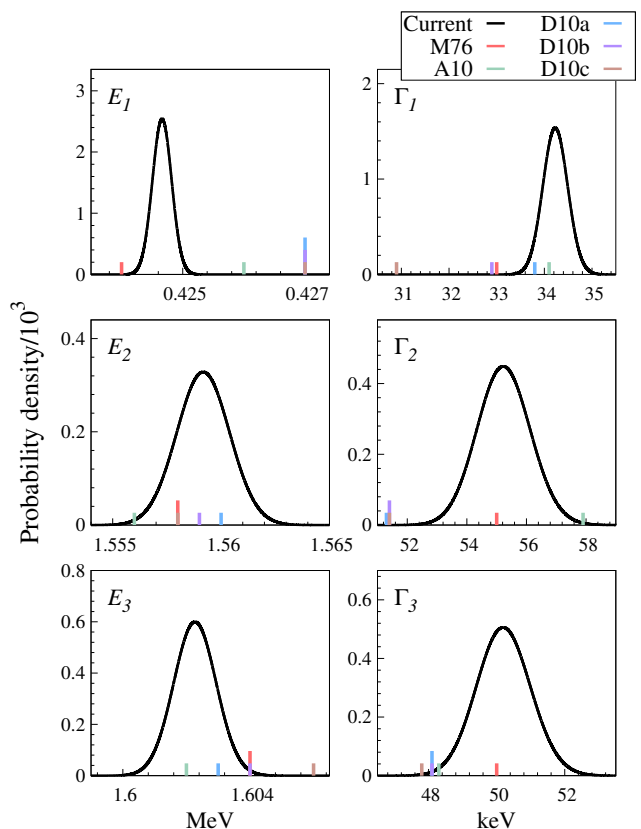


FIG. 4. Predictions of E and Γ on the measurement data. The references are presented by columns labeled with the first letter of the first author's last name followed by the last two numbers of the publication year [1, 16, 21]. Ref. [1] presented three results using different values of channel radius. These lognormal distributions are very close to Gaussian distributions.

training data or fine tuning model hyperparameters, this performance can be further improved if needed.

Fig. 3 shows a calibration of the prediction uncertainty. For discrete parameters J and π , the confidence level is the predicted probability from the softmax function, and the accuracy is the fraction of correct predictions. For continuous parameters E and Γ , the confidence levels are calculated from their predicted ranges surrounding their median values, and the accuracies are the fraction of true data points included in the corresponding ranges. The dashed black line shows the ideal case where the confidence level is equal to the accuracy. It is clear that our probabilistic model achieves a performance close to this ideal case.

Fig. 4 shows the model predictions on the measurement data of ref. [21], along with the previous results of R-matrix analyses on the same data to extract E and Γ [1, 16, 21]. Our predictions of the spin-parities of second and third states are, at $\sim 100\%$ probability, $J_2 = 3/2$, $\pi_2 = -$, and $J_3 = 5/2$, in agreement with the literature [35]. Our predictions of E and Γ extracted from the data are for the most part consistent with those of the

previous studies. These consistent results on the well-known reaction data demonstrate the effectiveness of our model. While the previous works used different channel radius values and background pole configurations, the determinations of those parameters are not made in the current work. Our results are also tabulated in Table II.

The current method is applicable to a wide variety of physics models. In this study, we focused on eliminating unobservable parameters, but this approach works for any subset of the parameters of a model. Interpolations or extrapolations of measured data are also possible by properly configuring the outputs of the deep learning model. Our approach of eliminating parameters could be used both when building generalized models that address a variety of problems, as well as when building pre-trained models that need only to be slightly adjusted for a specific task [23, 36].

The performance of the deep learning model can exceed that of the physics model for cases where the values of the unobservable parameters are unknown. The performance of the deep learning model closely resembles that of the physics model if these unobservables are (by some means) correctly specified. Specifically, the deep learning model can accurately extract distinctive features from the data, features that arise from variations of the observable parameters of the model. However, in cases where variations of unobservable parameters can impact these features, the deep learning model predictions will have high uncertainties. By adding more training data samples or fine-tuning the deep learning model, these uncertainties can be reduced [37–39].

There are some additional benefits of our deep learning approach beyond the elimination of unobservable parameters. First, once a deep learning model is trained, the prediction calculation is normally much faster than typical Bayesian inference approaches that require a large number of Monte Carlo samplings [9, 40, 41]. Second, as shown in Fig. 3, the confidence level of the uncertainties in the deep learning model predictions can be explicitly tested through an analysis of a subset of data (a test dataset) [29, 32, 42, 43].

The presence of unobservable parameters in physics models can, in some cases, lead to ambiguities in the extraction of observable parameters from measured data. We demonstrate that a deep learning model can be trained without specifying such unobservable parameters by extracting values of observables directly from features in the dataset. By training the deep learning model without information on unobservables, these parameters are effectively eliminated. We demonstrate the effectiveness of this method on the phenomenological R-matrix model using a deep learning model based on Transformers. We trained this model to directly extract, from $^{12}\text{C}+p$ scattering measurement data, values of the observable parameters – resonance energies, widths, spins, and parities – with no need to specify values of the unobservable channel radius and background pole parameters used in traditional R-matrix analyses. We performed un-

certainty quantification in deep learning using a probabilistic framework that provides calibrated uncertainties as tested on a subset of data samples. Our approach has broad applicability in physics to remove unobservables, or other subsets of model parameters, in analyzing datasets.

ACKNOWLEDGEMENTS

This work was supported by the National Research Foundation of Korea (NRF) grants funded by the Korea government (MSIT) (Grants No. 2016R1A5A1013277 and No. 2020R1A2C1005981). This work was also supported in part by the Institute for Basic Science (Grant No. IBS-R031-D1), and by the U.S. Dept. of Energy (DOE), Office of Science, Office of Nuclear Physics under contract DE-AC05-00OR22725. Computational works for this research were performed on the data analysis hub, Olaf in the IBS Research Solution Center.

METHODS

Data Preparation

To generate the training data, we set ranges of the resonance parameters where the true parameter values are possibly located. These ranges can be obtained from previous studies. Alternatively, one can assume physically probable ranges. For example, one knows that a reaction with a high l value is largely suppressed by the centrifugal barrier, which allows an assumption of a l value less than a particular number. These kinds of assumptions prevail in the conventional analysis, where one does not try fitting with every possible l value but only some that are practically probable.

Each set of parameters is used to calculate the corresponding cross section using the R-matrix code, AZURE2 [16]. The target measurement data has differential cross section values on certain energy bin points at three different angles [21]. The calculated cross section values on the same bin points at the three angles are taken as the input. As the locations of bin points and values of angles are fixed, they are null values in training and not included in the data. The input data samples are, therefore, 3-dimensional tensors with the shape of $(n_{\text{angle}}, n_{\text{bin}}, 1)$. n_{angle} is the number of measured angles, n_{bin} is the number of bin points, and 1 represents the value of the cross section. A cross section value corresponds to a word in the natural language processing using the Transformer (see the next section) [22].

We add random noises in the calculated cross section values assuming Gaussian noises to reflect the measurement noises. The standard deviations of the Gaussians are obtained from the measurement error bars in ref. [21]. The addition of measurement noises is flexible so that any type of noises can be added. Non-Gaussian noises

TABLE II. Predictions of E and Γ for the measurement data from ref. [21] along with the previous results [1, 16, 21]. For the current model, the median values of the distributions are presented with the standard deviations as representations.

Parameters	Current Model	Ref. [21] ¹	Ref. [16]	Ref. [1] ¹	Ref. [1] ¹	Ref. [1] ¹
E_1 (MeV)	0.4247(2)	0.424	0.426(3)	0.427	0.427	0.427
E_2 (MeV)	1.5592(12)	1.558	1.556(1)	1.560	1.559	1.558
E_3 (MeV)	1.6023(7)	1.604	1.602(2)	1.603	1.604	1.606
Γ_1 (keV)	34.2(3)	33	34.1(8)	33.8	32.9	30.9
Γ_2 (keV)	55.2(9)	55	57.9(17)	51.4	51.4	51.3
Γ_3 (keV)	50.2(8)	50	48.3(19)	48.1	48.1	47.8
a_c (fm)	-	4.0	3.4	4.0	5.0	6.0
Background Poles	-	$3/2^+$ state ²	3	3	3	3

¹ The uncertainties are not presented in the papers. ² While it was not explicitly stated as a background pole, the experimentally known $3/2^+$ level at $E = 5.860$ MeV with $\Gamma = 1400$ keV was included in the calculation in ref. [21]. ³ No background pole was considered.

or noise on measured energy points can be handled by simply adding such noises to the training data.

Model Architecture

The base architecture of the current model is from the Transformer [22]. Details of its description can be found in ref. [22]. Here, we briefly summarize its main features. The Transformer was originally constructed to handle sequence data for natural language processing. For translation purposes, the input and output are, for example, sentences from two different languages. The architecture is based on an encoder-decoder structure. Both encoder and decoder consist of multiple layers with multi-head attentions, fully connected feed-forward networks, residual connections, and layer normalizations [44, 45]. A multi-head attention splits the incoming data and performs multiple attention functions known as scaled dot-product attention to let the model attend the data points at multiple aspects [22]. An encoder layer contains a multi-head self-attention and feed-forward network. On the other hand, a decoder layer contains an additional multi-head attention performing with the encoder output, known as encoder-decoder attention.

The attentions find critical relations between two sequence data, known as a query and key, and use them to update another sequence data, known as a value. Queries, keys, and values in the self-attentions originate from the input. On the other hand, in the encoder-decoder attentions, queries originate from the decoder input, and keys and values originate from the encoder output. The obtained relations are often called atten-

tion (score) matrices, and they present locations of data points critical for the model predictions. Fig. 5 shows examples of the attention matrices from the current model in the prediction of the target measurement data.

The description of modifications to the original architecture is following. The inputs to the encoder and decoder are originally embedded and pass the positional encoding to convert the sentences to vectors and encode positional information of each word [22]. In this work, we remove such functions as the inputs are not exactly sentences but spectra with continuous values. We simply replace the embedding and positional encoding with a linear layer that projects a cross section point to a vector. After the first linear layer, the shape $(n_{\text{angle}}, n_{\text{bin}}, 1)$ is converted into $(n_{\text{angle}}, n_{\text{bin}}, d_{\text{model}})$, where d_{model} is a hyperparameter of the Transformer [22]. Additionally, we use the Gaussian Error Linear Units function as the activation function in the feed-forward networks [46].

The main operations in the Transformer are matrix multiplications that perform on the last two dimensions of data, whereas the current data has three dimensions. The decoder in the Transformer performs the multi-head attention between its input and the encoder output. We give the decoder input the same input as the encoder but shifted at the extra angle dimension, $[\theta_1, \theta_2, \theta_3] \rightarrow [\theta_3, \theta_1, \theta_2]$. By doing so, the matrix multiplications in the attention are done between the data of different angles. The decoder input does not require the look-ahead mask originally demanded by the Transformer that uses target sequences as decoder input.

The hyperparameters in the model are:

- $d_{\text{model}} = 256$

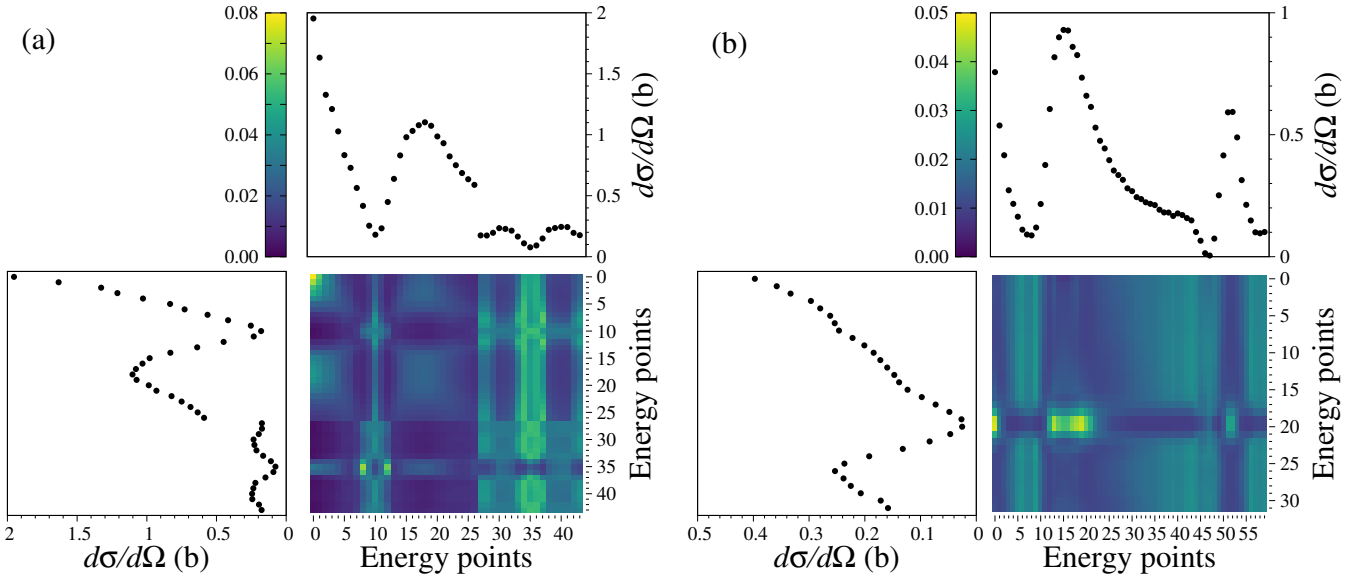


FIG. 5. Examples of the attention matrices when the target measurement data is passed as input. **a**, an attention matrix from self-attention in the decoder. **b**, an attention matrix from encoder-decoder attention. The top and left plots of each matrix show the corresponding input data. See text for the explanation of attentions.

- $d_{\text{ff}} = 256$
- $d_{\text{q}} = d_{\text{k}} = d_{\text{v}} = 32$
- $h = 8$
- The number of encoder layers = 2
- The number of decoder layers = 2

We followed the notation of ref. [22].

The output of the modified Transformer is reshaped and passed to linear layers at the end of the model to return the four types of parameters.

Probabilistic Model

We utilize a probabilistic framework to estimate the uncertainties of the model predictions. The method of deep ensembles is one of the most practical and effective uncertainty quantification approaches [29–31]. Deep ensembles consist of N_{model} point-estimate models trained with random initialization of model parameters and shuffling of data samples. In this study, we used 5 point-estimate models, $N_{\text{model}} = 5$. While it was first proposed as a non-Bayesian neural network, it has been shown that this method can be viewed as another Bayesian approach [29, 31, 47, 48]. Bayesian deep learning critically uses marginalization over possible sets of model parameters to obtain the predictive distribution [29, 48]:

$$p(\mathbf{y} | \mathbf{x}, \mathbf{D}) = \int_{\theta} p(\mathbf{y} | \mathbf{x}, \theta') p(\theta' | \mathbf{D}) d\theta', \quad (2)$$

where \mathbf{x} and \mathbf{y} represents input and prediction, θ represents the model parameters, and \mathbf{D} represents training data. The prediction of deep ensembles in Equation 1 is equivalent to Equation 2 if the posterior is a mixture of delta functions. For this reason, deep ensembles can be seen as Bayesian marginalization with variational inference via a mixture of delta functions for the approximate distribution, $p(\theta | \mathbf{D}) \sim q_{\phi}(\theta) = (1/N_{\text{model}}) \sum_{p=1}^{N_{\text{model}}} \delta(\theta = \theta_p)$. One of the advantages of deep ensembles is that they can capture different modes of posterior as multiple models are optimized to different optima [29, 47, 48]. More details on deep ensembles can be found in refs. [29, 31, 48].

We use negative log-likelihood (NLL) for the loss function in training. For regression, NLL for a data point i is

$$\begin{aligned} \text{NLL} &= -\log p(y_i | f_{\text{NN}}(\mathbf{x}_i; \theta)) \\ &= \frac{1}{2\sigma(\mathbf{x}_i; \theta)^2} \|y_i - \mu(\mathbf{x}_i; \theta)\|^2 \\ &\quad + \frac{1}{2} \log(2\pi\sigma(\mathbf{x}_i; \theta)^2), \end{aligned} \quad (3)$$

where f_{NN} represents the neural network. The mean μ and standard deviation σ are predicted by the neural network with the model parameter θ and input \mathbf{x}_i . For classification, we also implement the method proposed by ref. [38]. They presented a framework to combine aleatoric and epistemic uncertainties and showed the robustness of the method [37–39]. Logit vectors are sampled from a Gaussian distribution whose mean and standard deviation are predicted by the model. After passing them to a softmax function, the average of the softmax outputs is used to calculate NLL. For these reasons, the model

in the current study has two outputs, μ and σ , for each parameter prediction.

We performed the training for 4,200 epochs with $\sim 21,000$ training samples and $\sim 5,000$ validation samples. The batch size was 768 on 3 GPU workers (NVIDIA Tesla V100 32GB SXM2). The number of samples is free to increase at the expense of training time. We used Adam optimizer with a weight decay of 10^{-9} [49]. The learning rate was 0.0002 with a scheduler that decreased the learning rate by a factor of 0.99 at every 6 epochs. We constantly monitored the mean errors of predictions and NLL. After the training, we test the model with a relatively large number of samples, $\sim 30,000$, to plot a reli-

ability diagram with enough number of sample in each bin.

We plot the reliability diagram for the performance test of the probabilistic model. For the classification tasks, the predicted probabilities are not evenly distributed to all probability ranges because of the high accuracies. For this reason, we set the bin locations to have an equal number of samples in each bin, not to have an equal bin interval. For regression tasks, we span the ranges from the median that corresponds to the mean of the original Gaussian $N(\mu, \sigma^2)$; for example, from $e^{\mu-\sigma}$ to $e^{\mu+\sigma}$ for 68% confidence interval.

-
- [1] P. Descouvemont, D. Baye, The R-matrix theory, Reports on Progress in Physics 73 (3) (2010) 036301. [arXiv:1001.0678](https://arxiv.org/abs/1001.0678), [doi:10.1088/0034-4885/73/3/036301](https://doi.org/10.1088/0034-4885/73/3/036301).
- [2] M. Baldo, G. F. Burgio, The nuclear symmetry energy, Progress in Particle and Nuclear Physics 91 (2016) 203–258. [arXiv:1606.08838](https://arxiv.org/abs/1606.08838), [doi:10.1016/j.ppnp.2016.06.006](https://doi.org/10.1016/j.ppnp.2016.06.006).
- [3] R. J. deBoer, J. Görres, M. Wiescher, R. E. Azuma, A. Best, C. R. Brune, C. E. Fields, S. Jones, M. Pignatari, D. Sayre, K. Smith, F. X. Timmes, E. Uberseder, The $^{12}\text{C}(\alpha, \gamma)^{16}\text{O}$ reaction and its implications for stellar helium burning, Reviews of Modern Physics 89 (3) (2017) 035007. [arXiv:1709.03144](https://arxiv.org/abs/1709.03144), [doi:10.1103/RevModPhys.89.035007](https://doi.org/10.1103/RevModPhys.89.035007).
- [4] B. S. Rem, N. Käming, M. Tarnowski, L. Asteria, N. Fläschner, C. Becker, K. Sengstock, C. Weitenberg, Identifying quantum phase transitions using artificial neural networks on experimental data, Nature Physics 15 (9) (2019) 917–920. [arXiv:1809.05519](https://arxiv.org/abs/1809.05519), [doi:10.1038/s41567-019-0554-0](https://doi.org/10.1038/s41567-019-0554-0).
- [5] L. G. Wright, T. Onodera, M. M. Stein, T. Wang, D. T. Schachter, Z. Hu, P. L. McMahon, Deep physical neural networks trained with backpropagation, Nature 601 (7894) (2022) 549–555. [doi:10.1038/s41586-021-04223-6](https://doi.org/10.1038/s41586-021-04223-6).
- [6] F. Ashtiani, A. J. Geers, F. Aflatouni, An on-chip photonic deep neural network for image classification, Nature 606 (7914) (2022) 501–506. [arXiv:2106.11747](https://arxiv.org/abs/2106.11747), [doi:10.1038/s41586-022-04714-0](https://doi.org/10.1038/s41586-022-04714-0).
- [7] C. H. Kim, S. Ahn, K. Y. Chae, J. Hooker, G. V. Rogachev, Noise signal identification in time projection chamber data using deep learning model, Nuclear Instruments and Methods in Physics Research Section A: Accelerators, Spectrometers, Detectors and Associated Equipment 1048 (2023) 168025. [doi:https://doi.org/10.1016/j.nima.2023.168025](https://doi.org/10.1016/j.nima.2023.168025).
- [8] C. H. Kim, S. Ahn, K. Y. Chae, J. Hooker, G. V. Rogachev, Restoring original signal from pile-up signal using deep learning (2023). [arXiv:2304.14496](https://arxiv.org/abs/2304.14496).
- [9] H. Gabbard, C. Messenger, I. S. Heng, F. Tonolini, R. Murray-Smith, Bayesian parameter estimation using conditional variational autoencoders for gravitational-wave astronomy, Nature Physics 18 (1) (2022) 112–117. [arXiv:1909.06296](https://arxiv.org/abs/1909.06296), [doi:10.1038/s41567-021-01425-7](https://doi.org/10.1038/s41567-021-01425-7).
- [10] A. W. Senior, R. Evans, J. Jumper, J. Kirkpatrick, L. Sifre, T. Green, C. Qin, A. Židek, A. W. R. Nelson, A. Bridgland, H. Penedones, S. Petersen, K. Simonyan, S. Crossan, P. Kohli, D. T. Jones, D. Silver, K. Kavukcuoglu, D. Hassabis, Improved protein structure prediction using potentials from deep learning, Nature 577 (7792) (2020) 706–710. [doi:10.1038/s41586-019-1923-7](https://doi.org/10.1038/s41586-019-1923-7).
- [11] J. Jumper, R. Evans, A. Pritzel, T. Green, M. Figurnov, O. Ronneberger, K. Tunyasuvunakool, R. Bates, A. Židek, A. Potapenko, A. Bridgland, C. Meyer, S. A. A. Kohl, A. J. Ballard, A. Cowie, B. Romera-Paredes, S. Nikolov, R. Jain, J. Adler, T. Back, S. Petersen, D. Reiman, E. Clancy, M. Zielinski, M. Steinegger, M. Pacholska, T. Berghammer, S. Bodenstein, D. Silver, O. Vinyals, A. W. Senior, K. Kavukcuoglu, P. Kohli, D. Hassabis, Highly accurate protein structure prediction with AlphaFold, Nature 596 (7873) (2021) 583–589. [doi:10.1038/s41586-021-03819-2](https://doi.org/10.1038/s41586-021-03819-2).
- [12] M. Raissi, P. Perdikaris, G. E. Karniadakis, Physics-informed neural networks: A deep learning framework for solving forward and inverse problems involving nonlinear partial differential equations, Journal of Computational Physics 378 (2019) 686–707. [doi:10.1016/j.jcp.2018.10.045](https://doi.org/10.1016/j.jcp.2018.10.045).
- [13] A. M. Lane, R. G. Thomas, R-Matrix Theory of Nuclear Reactions, Reviews of Modern Physics 30 (2) (1958) 257–353. [doi:10.1103/RevModPhys.30.257](https://doi.org/10.1103/RevModPhys.30.257).
- [14] G. M. Hale, R. E. Brown, N. Jarmie, Pole structure of the $J^\pi=3/2^+$ resonance in ^5He , Physical Review Letters 59 (7) (1987) 763–766. [doi:10.1103/PhysRevLett.59.763](https://doi.org/10.1103/PhysRevLett.59.763).
- [15] H. O. U. Fynbo, C. A. Diget, U. C. Bergmann, M. J. G. Borge, J. Cederkäll, P. Dendooven, L. M. Fraile, S. Franchoo, V. N. Fedosseev, B. R. Fulton, W. Huang, J. Huikari, H. B. Jeppesen, A. S. Jokinen, P. Jones, B. Jonson, U. Köster, K. Langanke, M. Meister, T. Nilsson, G. Nyman, Y. Prezado, K. Riisager, S. Rinta-Antila, O. Tengblad, M. Turrion, Y. Wang, L. Weissman, K. Wilhelmsen, J. Äystö, ISOLDE Collaboration, Revised rates for the stellar triple- α process from measurement of ^{12}C nuclear resonances, Nature 433 (7022) (2005) 136–139.
- [16] R. E. Azuma, E. Uberseder, E. C. Simpson, C. R. Brune, H. Costantini, R. J. de Boer, J. Görres, M. Heil, P. J. Leblanc, C. Ugalde, M. Wiescher, AZURE: An R-matrix

- code for nuclear astrophysics, *Physical Review C* 81 (4) (2010) 045805. [doi:10.1103/PhysRevC.81.045805](https://doi.org/10.1103/PhysRevC.81.045805).
- [17] E. G. Adelberger, A. García, R. G. H. Robertson, K. A. Snover, A. B. Balantekin, K. Heeger, M. J. Ramsey-Musolf, D. Bemmerer, A. Junghans, C. A. Bertulani, J. W. Chen, H. Costantini, P. Prati, M. Couder, E. Uberseder, M. Wiescher, R. Cyburt, B. Davids, S. J. Freedman, M. Gai, D. Gazit, L. Gialanella, G. Imbriani, U. Greife, M. Hass, W. C. Haxton, T. Itahashi, K. Kubodera, K. Langanke, D. Leitner, M. Leitner, P. Vetter, L. Winslow, L. E. Marcucci, T. Motobayashi, A. Mukhamedzhanov, R. E. Tribble, K. M. Nollett, F. M. Nunes, T. S. Park, P. D. Parker, R. Schiavilla, E. C. Simpson, C. Spitaleri, F. Strieder, H. P. Trautvetter, K. Suemmerer, S. Typel, Solar fusion cross sections. II. The pp chain and CNO cycles, *Reviews of Modern Physics* 83 (1) (2011) 195–246. [arXiv:1004.2318](https://arxiv.org/abs/1004.2318), [doi:10.1103/RevModPhys.83.195](https://doi.org/10.1103/RevModPhys.83.195).
- [18] A. Tumino, C. Spitaleri, M. La Cognata, S. Cherubini, G. L. Guardo, M. Gulino, S. Hayakawa, I. Indelicato, L. Lamia, H. Petrascu, R. G. Pizzone, S. M. R. Puglia, G. G. Rapisarda, S. Romano, M. L. Sergi, R. Spartá, L. Trache, An increase in the $^{12}\text{C} + ^{12}\text{C}$ fusion rate from resonances at astrophysical energies, *Nature* 557 (7707) (2018) 687–690. [doi:10.1038/s41586-018-0149-4](https://doi.org/10.1038/s41586-018-0149-4).
- [19] J. Bishop, C. E. Parker, G. V. Rogachev, S. Ahn, E. Koshchiy, K. Brandenburg, C. R. Brune, R. J. Charity, J. Derkin, N. Dronchi, G. Hamad, Y. Jones-Alberty, T. Kokalova, T. N. Massey, Z. Meisel, E. V. Ohstrom, S. N. Paneru, E. C. Pollacco, M. Saxena, N. Singh, R. Smith, L. G. Sobotka, D. Soltész, S. K. Subedi, A. V. Voinov, J. Warren, C. Wheldon, Neutron-upscattering enhancement of the triple-alpha process, *Nature Communications* 13 (2022) 2151. [doi:10.1038/s41467-022-29848-7](https://doi.org/10.1038/s41467-022-29848-7).
- [20] S. Artemov, E. Zapparov, G. Nie, Asymptotic normalization factors for light nuclei from proton transfer reactions, *Bulletin of the Russian Academy of Sciences-Physics* 67 (11) (2003) 1741–1746.
- [21] H. O. Meyer, G. R. Plattner, I. Sick, Elastic $p+^{12}\text{C}$ scattering between 0.3 and 2 MeV, *Zeitschrift für Physik A Hadrons and Nuclei* 279 (1) (1976) 41–45. [doi:10.1007/BF01409090](https://doi.org/10.1007/BF01409090).
- [22] A. Vaswani, N. Shazeer, N. Parmar, J. Uszkoreit, L. Jones, A. N. Gomez, L. Kaiser, I. Polosukhin, Attention Is All You Need, *arXiv e-prints* (2017) [arXiv:1706.03762](https://arxiv.org/abs/1706.03762) [arXiv:1706.03762](https://arxiv.org/abs/1706.03762).
- [23] J. Devlin, M.-W. Chang, K. Lee, K. Toutanova, BERT: Pre-training of Deep Bidirectional Transformers for Language Understanding, *arXiv e-prints* (2018) [arXiv:1810.04805](https://arxiv.org/abs/1810.04805) [arXiv:1810.04805](https://arxiv.org/abs/1810.04805).
- [24] D. W. Otter, J. R. Medina, J. K. Kalita, A Survey of the Usages of Deep Learning in Natural Language Processing, *arXiv e-prints* (2018) [arXiv:1807.10854](https://arxiv.org/abs/1807.10854) [arXiv:1807.10854](https://arxiv.org/abs/1807.10854).
- [25] Z. Liu, Y. Lin, Y. Cao, H. Hu, Y. Wei, Z. Zhang, S. Lin, B. Guo, Swin Transformer: Hierarchical Vision Transformer using Shifted Windows, *arXiv e-prints* (2021) [arXiv:2103.14030](https://arxiv.org/abs/2103.14030) [arXiv:2103.14030](https://arxiv.org/abs/2103.14030), [doi:10.48550/arXiv.2103.14030](https://doi.org/10.48550/arXiv.2103.14030).
- [26] S. Khan, M. Naseer, M. Hayat, S. Waqas Zamir, F. Shahbaz Khan, M. Shah, Transformers in Vision: A Survey, *arXiv e-prints* (2021) [arXiv:2101.01169](https://arxiv.org/abs/2101.01169) [arXiv:2101.01169](https://arxiv.org/abs/2101.01169), [doi:10.48550/arXiv.2101.01169](https://doi.org/10.48550/arXiv.2101.01169).
- [27] N. Wu, B. Green, X. Ben, S. O'Banion, Deep Transformer Models for Time Series Forecasting: The Influenza Prevalence Case, *arXiv e-prints* (2020) [arXiv:2001.08317](https://arxiv.org/abs/2001.08317) [arXiv:2001.08317](https://arxiv.org/abs/2001.08317), [doi:10.48550/arXiv.2001.08317](https://doi.org/10.48550/arXiv.2001.08317).
- [28] H. Zhou, S. Zhang, J. Peng, S. Zhang, J. Li, H. Xiong, W. Zhang, Informer: Beyond Efficient Transformer for Long Sequence Time-Series Forecasting, *arXiv e-prints* (2020) [arXiv:2012.07436](https://arxiv.org/abs/2012.07436) [arXiv:2012.07436](https://arxiv.org/abs/2012.07436), [doi:10.48550/arXiv.2012.07436](https://doi.org/10.48550/arXiv.2012.07436).
- [29] L. Valentin Jospin, W. Buntine, F. Boussaid, H. Laga, M. Bennamoun, Hands-on Bayesian Neural Networks – a Tutorial for Deep Learning Users, *arXiv e-prints* (2020) [arXiv:2007.06823](https://arxiv.org/abs/2007.06823) [arXiv:2007.06823](https://arxiv.org/abs/2007.06823).
- [30] K. P. Murphy, Probabilistic machine learning: an introduction, MIT press, 2022.
- [31] B. Lakshminarayanan, A. Pritzel, C. Blundell, Simple and Scalable Predictive Uncertainty Estimation using Deep Ensembles, *arXiv e-prints* (2016) [arXiv:1612.01474](https://arxiv.org/abs/1612.01474) [arXiv:1612.01474](https://arxiv.org/abs/1612.01474), [doi:10.48550/arXiv.1612.01474](https://doi.org/10.48550/arXiv.1612.01474).
- [32] Y. Ovadia, E. Fertig, J. Ren, Z. Nado, D. Sculley, S. Nowozin, J. Dillon, B. Lakshminarayanan, J. Snoek, Can you trust your model's uncertainty? evaluating predictive uncertainty under dataset shift, in: H. Wallach, H. Larochelle, A. Beygelzimer, F. d'Alché-Buc, E. Fox, R. Garnett (Eds.), *Advances in Neural Information Processing Systems*, Vol. 32, Curran Associates, Inc., 2019.
- [33] M. Abdar, F. Pourpanah, S. Hussain, D. Reza-zadegan, L. Liu, M. Ghavamzadeh, P. Fieguth, X. Cao, A. Khosravi, U. Rajendra Acharya, V. Makarenkov, S. Nahavandi, A Review of Uncertainty Quantification in Deep Learning: Techniques, Applications and Challenges, *arXiv e-prints* (2020) [arXiv:2011.06225](https://arxiv.org/abs/2011.06225) [arXiv:2011.06225](https://arxiv.org/abs/2011.06225), [doi:10.48550/arXiv.2011.06225](https://doi.org/10.48550/arXiv.2011.06225).
- [34] R. Longland, C. Iliadis, A. E. Champagne, J. R. Newton, C. Ugalde, A. Coc, R. Fitzgerald, Charged-particle thermonuclear reaction rates: I. Monte Carlo method and statistical distributions, *Nuclear Physics A* 841 (1-4) (2010) 1–30. [arXiv:1004.4136](https://arxiv.org/abs/1004.4136), [doi:10.1016/j.nuclphysa.2010.04.008](https://doi.org/10.1016/j.nuclphysa.2010.04.008).
- [35] F. Ajzenberg-Selove, Energy levels of light nuclei $a = 13-15$, *Nuclear Physics A* 523 (1) (1991) 1–196. [doi:https://doi.org/10.1016/0375-9474\(91\)90446-D](https://doi.org/10.1016/0375-9474(91)90446-D).
- [36] F. Zhuang, Z. Qi, K. Duan, D. Xi, Y. Zhu, H. Zhu, H. Xiong, Q. He, A comprehensive survey on transfer learning, *Proceedings of the IEEE* 109 (1) (2021) 43–76. [doi:10.1109/JPROC.2020.3004555](https://doi.org/10.1109/JPROC.2020.3004555).
- [37] A. Der Kiureghian, O. Ditlevsen, Aleatory or epistemic? does it matter?, *Structural safety* 31 (2) (2009) 105–112.
- [38] A. Kendall, Y. Gal, What uncertainties do we need in bayesian deep learning for computer vision?, *CoRR abs/1703.04977* (2017). [arXiv:1703.04977](https://arxiv.org/abs/1703.04977).
- [39] E. Hüllermeier, W. Waegeman, Aleatoric and Epistemic Uncertainty in Machine Learning: An Introduction to Concepts and Methods, *arXiv e-prints* (2019) [arXiv:1910.09457](https://arxiv.org/abs/1910.09457) [arXiv:1910.09457](https://arxiv.org/abs/1910.09457), [doi:10.48550/arXiv.1910.09457](https://doi.org/10.48550/arXiv.1910.09457).
- [40] U. von Toussaint, Bayesian inference in physics, *Reviews of Modern Physics* 83 (3) (2011) 943–999. [doi:10.1103/RevModPhys.83.943](https://doi.org/10.1103/RevModPhys.83.943).
- [41] A. J. K. Chua, M. Vallisneri, Learning Bayesian

- Posteriors with Neural Networks for Gravitational-Wave Inference, *Physical Review Letters* 124 (4) (2020) 041102. [arXiv:1909.05966](https://arxiv.org/abs/1909.05966), [doi:10.1103/PhysRevLett.124.041102](https://doi.org/10.1103/PhysRevLett.124.041102).
- [42] A. P. Dawid, The well-calibrated bayesian, *Journal of the American Statistical Association* 77 (379) (1982) 605–610. [arXiv:https://www.tandfonline.com/doi/pdf/10.1080/01621459.1982.10477856](https://arxiv.org/abs/https://www.tandfonline.com/doi/pdf/10.1080/01621459.1982.10477856), [doi:10.1080/01621459.1982.10477856](https://doi.org/10.1080/01621459.1982.10477856).
- [43] C. Guo, G. Pleiss, Y. Sun, K. Q. Weinberger, **On calibration of modern neural networks**, in: D. Precup, Y. W. Teh (Eds.), *Proceedings of the 34th International Conference on Machine Learning*, Vol. 70 of *Proceedings of Machine Learning Research*, PMLR, 2017, pp. 1321–1330. URL <https://proceedings.mlr.press/v70/guo17a.html>
- [44] K. He, X. Zhang, S. Ren, J. Sun, Deep Residual Learning for Image Recognition, *arXiv e-prints* (2015) [arXiv:1512.03385](https://arxiv.org/abs/1512.03385)[arXiv:1512.03385](https://arxiv.org/abs/1512.03385), [doi:10.48550/arXiv.1512.03385](https://doi.org/10.48550/arXiv.1512.03385).
- [45] J. Lei Ba, J. R. Kiros, G. E. Hinton, Layer Normalization, *arXiv e-prints* (2016) [arXiv:1607.06450](https://arxiv.org/abs/1607.06450)[arXiv:1607.06450](https://arxiv.org/abs/1607.06450), [doi:10.48550/arXiv.1607.06450](https://doi.org/10.48550/arXiv.1607.06450).
- [46] D. Hendrycks, K. Gimpel, Gaussian Error Linear Units (GELUs), *arXiv e-prints* (2016) [arXiv:1606.08415](https://arxiv.org/abs/1606.08415)[arXiv:1606.08415](https://arxiv.org/abs/1606.08415), [doi:10.48550/arXiv.1606.08415](https://doi.org/10.48550/arXiv.1606.08415).
- [47] F. K. Gustafsson, M. Danelljan, T. B. Schön, Evaluating Scalable Bayesian Deep Learning Methods for Robust Computer Vision, *arXiv e-prints* (2019) [arXiv:1906.01620](https://arxiv.org/abs/1906.01620)[arXiv:1906.01620](https://arxiv.org/abs/1906.01620), [doi:10.48550/arXiv.1906.01620](https://doi.org/10.48550/arXiv.1906.01620).
- [48] A. G. Wilson, P. Izmailov, Bayesian deep learning and a probabilistic perspective of generalization, *CoRR abs/2002.08791* (2020). [arXiv:2002.08791](https://arxiv.org/abs/2002.08791).
- [49] D. P. Kingma, J. Ba, Adam: A Method for Stochastic Optimization, *arXiv e-prints* (2014) [arXiv:1412.6980](https://arxiv.org/abs/1412.6980).